RF-MAC: A Medium Access Control Protocol for Re-Chargeable Sensor Networks Powered by Wireless Energy Harvesting

M. Yousof Naderi, *Member, IEEE*, Prusayon Nintanavongsa, *Member, IEEE*, and Kaushik R. Chowdhury, *Member, IEEE*

***Abstract*—Wireless charging through directed radio frequency (RF) waves is an emerging technology that can be used to replenish the battery of a sensor node, albeit at the cost of data communication in the network. This tradeoff between energy transfer and communication functions requires a fresh perspective on medium access control (MAC) protocol design for appropriately sharing the channel. Through an experimental study, we demonstrate how the placement, the chosen frequency, and number of the RF energy transmitters impact the sensor charging time. These studies are then used to design a MAC protocol called RF-MAC that optimizes energy delivery to sensor nodes, while minimizing disruption to data communication. In the course of the protocol design, we describe mechanisms for (i) setting the maximum energy charging threshold, (ii) selecting specific transmitters based on the collective impact on charging time, (iii) requesting and granting energy transfer requests, and (iv) evaluating the respective priorities of data communication and energy transfer. To the best of our knowledge, this is the first distributed MAC protocol for RF energy harvesting sensors, and through a combination of experimentation and simulation studies, we observe 300% maximum network throughput improvement over the classical modified unslotted CSMA MAC protocol.**

***Index Terms*—Medium access protocol, optimization, RF harvesting, sensor networks, wireless power transfer.**

I. Introduction

WIRELESS SENSOR NETWORKs (WSNs) are being increasingly used in a wide variety of applications including industrial and infrastructure monitoring, smart home, smart grid, medical systems, and so on. One of the main challenges and performance bottleneck in these systems is the limited lifetime of the sensor nodes due to their energy supply. Recent advances in the area of wireless energy transfer allow sensors to recharge during network operation, thereby extending their lifetimes and minimizing application downtime. Our recent research on powering Mica2 sensor motes by harvesting the energy contained in radio frequency (RF) electromagnetic waves in [1] indicated the potential for large scale deployment of this technology. However, at the protocol level, this form of in-band energy replenishment is fraught with several challenges on: (i) how and when should the energy transfer occur, (ii) its priority over, and the resulting impact on the process of data communication, (iii) the challenges in aggregating the charging action of multiple transmitters, and (iv) impact of the choice of frequency. Thus, the act of energy transfer becomes a complex medium access problem, which must embrace a cross-disciplinary approach incorporating wave propagation effects and device characteristics, apart from the classical link layer problem of achieving fairness in accessing the channel. We focus on in-band transmission since multiple separate frequencies for data and energy transfer increases the complexity of the sensors, brings in numerous antennas and transceiver related hardware requirements, and imposes additional spectrum availability needs. This paper is concerned with the design of a CSMA/CA based MAC protocol for such RF energy harvesting sensors, inspired by experimental evaluations on our testbed.

Our MAC protocol that works with RF energy harvesting, called as RF-MAC, allows a node to broadcast its request for energy (RFE) packet containing its ID, and then waits to hear from the energy transmitters (ETs) in the neighborhood. These responses from ETs are called cleared for energy (CFE) pulses, which are simple, time-separated energy beacons. These pulses maybe transmitted by more than one ET concurrently as overlapping CFEs need not be distinguished. Rather, the concurrent emission of the CFEs increases the received energy level at the sensor, and this indicates a higher number of potential transmitters from the energy requesting sensor. The responding ETs are then classified into two sets, based on rough estimates of their separation distance from the energy requesting node to minimize the impact of destructive interference as much as possible. Each set of ETs is assigned a slightly different peak transmission frequency (separated by only few KHz, hence, still called in-band as the channel separation is typically 5 MHz for 802.11) so that each set of ETs contributes constructively to the level of RF energy received at the node.

While we retain the essential concepts of the CSMA/CA mechanism for the data access mechanism [3], there are several points of departure from the classical implementation. We separately select and dynamically vary the slot time, the inter-frame

Manuscript received June 23, 2013; revised December 28, 2013; accepted March 17, 2014. Date of publication April 2, 2014; date of current version July 8, 2014. This work was supported by the U.S. National Science Foundation under Grant CNS-1143681. The associate editor coordinating the review of this paper and approving it for publication was P. Wang.

M. Y. Naderi and K. R. Chowdhury are with the Department of Electrical and Computer Engineering, Northeastern University, Boston, MA 02115 USA (e-mail: naderi@ece.neu.edu; krc@ece.neu.edu).

P. Nintanavongsa is with the Department of Computer Engineering, Rajamangala University of Technology Thanyaburi, Pathumtani 12110, Thailand (e-mail: prusayon.n@en.rmutt.ac.th).

Color versions of one or more of the figures in this paper are available online at http://ieeexplore.ieee.org.

Digital Object Identifier 10.1109/TWC.2014.2315211

spacing, and the contention window size for both energy transfer and data communication.

The core contributions of our work can be summarized as follows:

- We experimentally identify the operating constraints of the RF energy transferring MAC protocol using actual wireless energy harvesting circuits interfaced with Mica2 motes. We demonstrate how two slightly separated energy transfer frequencies can be assigned to ETs to improve the constructive interference of their collective action.
- We design a MAC protocol to balance the needs of efficient wireless energy delivery and data exchange. We bridge these dissimilar concepts by establishing the importance of a node in the data communication, which in turn quantifies how much should the node charge.
- We analytically establish optimality conditions for the energy transfer, and create a strongly coupled protocol that operates on link layer metrics with the awareness of both the underlying hardware and fundamental limits of RF energy harvesting.

The rest of this paper is organized as follows: In Section II, we give the related work. The key design challenges are described in Section III with experimental studies. A brief overview of our RF-MAC protocol in given in Section IV, with a comprehensive detailed description in Section V. The simulation and experimental results are presented in Sections VI and VII, respectively. Finally, Section VIII concludes our work.

II. Related Work

MAC protocols that aim for energy conservation have been extensively explored in the recent past, with a comprehensive classification and survey on this topic presented in [4], [14], [16], [19]. In this section, we review the related MAC protocols for energy harvesting sensor networks.

A. General Energy Harvesting Sensor Networks

In [17], the authors propose an on-demand medium access protocol (ODMAC) based on three basic ideas: minimizing wasting energy by moving the idle listening time from the receiver to the transmitter, adapting the duty cycle of the node to operate in the energy neutral operation (ENO) state (i.e., energy used by the system is less than the energy harvested from the environment), and reducing the end-to-end delay by employing an opportunistic forwarding scheme. In [4], a polling-based medium access mechanism (PP-MAC) is described for single-hop sensor networks, which uses the charge-and-spend paradigm for harvesting strategy. In [15], we model a CSMA-based MAC protocol with an ARQ error control mechanism for energy harvesting sensor networks through an analytical framework leveraging stochastic semi-Markov models. However, all of the above protocols assume no impact of the energy harvesting process on data communication.

B. Sensor Networks With Wireless Energy Transfer

Specific to the scenario of RF energy transfer, an energy-adaptive MAC protocol (EA-MAC) is proposed in [6], which adopts a duty-cycle based on the proportion of harvested energy. However, this protocol requires a strict centralized base station control and relies on out-of-band RF power transfer. In [7], conventional MAC protocols, such as the classical TDMA and variants of ALOHA are evaluated assuming out-of-band RF transfer.

In [8], the authors present multiple concepts for multi-hop wireless energy transfer (such as store and forward vs. directly single hop transfer) and derive the efficiency of each method using magnetically coupled resonators for wireless power transfer demonstrated in [13]. However, this non-radiative transfer is shown to work up to 2 m and requires perfectly aligned coils of 25 cm radius among the source and receiver nodes.

RFID technology comes closest to the energy transferring paradigm, where a tag operates using the incident RF power emitted by the transmitter [9]. The Token-MAC protocol for RFID systems in [12] enables fair access to the medium for all tags requiring neither a-priori knowledge of the tags nor synchronization. However, there are limitations in directly porting these approaches to networking scenarios, since RFID is unable to generate enough energy to run the local processing tasks on a typical node.

Some preliminary work on the energy transmitter grouping strategy appeared in [5], which has been integrated in the current RF-MAC protocol design.

III. Design Challenges and Preliminary Experiments

In this section we describe the key challenges for RF-MAC that concern specific characteristics of RF harvesting sensor networks, including (i) energy interference between emitted energy waves that results in wireless charging cancellation, (ii) optimal frequency and distance separation between ETs, (iii) energy charging time, (iv) requesting and granting energy, and (v) data vs. energy channel access.

A. Energy Interference and Cancellation

When more than one ET transmits power in-band, the concurrent emitted energy waves can combine either constructively or destructively, leading to variations in the amount of harvestable power and a possible energy cancellation. In the case of constructive interference (in-phase), the received power of the resulting wave at the RF energy harvester is greater than that of either of the individual energy waves. Conversely, in the case of destructive interference (out-phase), the net received power is less than that of the individual energy waves. This raises the question of which sets of ETs must be concurrently allowed to transmit by the MAC protocol, which we answer below.

An example network architecture, with stationary, omnidirectional ETs x, y, and z, is shown in Fig. 1(a). The sensor $S1$ can be charged either through a unilateral action of any of the ETs, or through a coordinated transmission of multiple ETs. However, the joint action can only be beneficial if the arriving waves at sensor $S1$ are aligned in phase. Hence, ETs x and z may together transmit, both being at a multiple of the signal wavelength λ away (which translates in a phase difference that results in 'constructive' interference). While the sensor can also

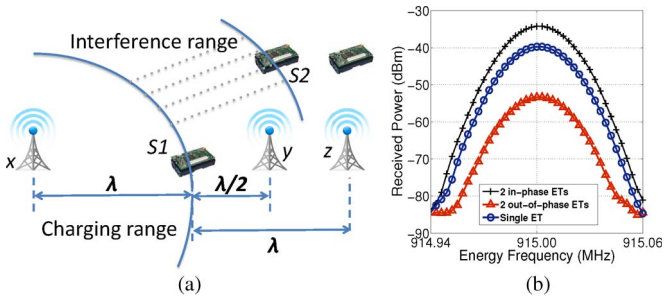

Fig. 1. Example network architecture with energy transmitters (x, y, z) and RF harvesting sensors $(S1, S2)$. The energy transmitters can cancel emitted energy waves of each others (a). Phase difference effect on the received signal power at 915 MHz (b).

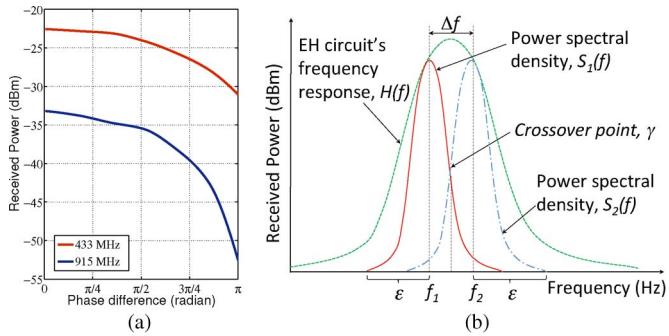

Fig. 2. Effect of energy waves phase difference on the received signal power at different frequencies. The power of the resulting wave drops significantly after $\pi/2$ phase separation (a). The scheme for two-tone wireless energy transfer (b).

be charged by ET y, combining the action of y with either of the others diminishes the performance (owing to y causing 'destructive' interference with respect to x and z).

To characterize the constructive and the destructive effect of the ETs, our experimental setup involved two such 0 dBm continuous wave transmitters, each placed 2.5 m on either side of the receiver. Two Agilent N5181 MXG RF signal generators, each connected to a 50 Ω omnidirectional antenna tuned to the 915 MHz ISM band, were used to generate the RF energy signal. We fixed the phase of one signal generator and varied the phase of another, while keeping their locations fixed (note that keeping the transmission phase fixed and varying their distance as a function of the signal wavelength will have the same effect on the received signal phase). The fall in the signal strength, shown in Fig. 1(b), was dramatic when the ETs operated in phase opposition (-54 dBm) compared to in-phase operation (-36 dBm). These results show the importance of considering such energy interferences when controlling the medium access in wireless-powered sensor networks.

Our observations motivate the design goal for our MAC protocol to ensure that the maximum energy transfer occurs by minimizing this cancellation effect, especially, in a shared medium where N energy transmitters may transmit on the channel at the same time.

B. Optimal Frequency and Distance Separation

We next find the optimal frequency separation of the continuous wave ETs and their respective distances from the energy requesting sensor. Our RF-MAC protocol will use these results in setting the transmission frequency and activating only those ETs that result in out-phase energy transfer. Our approach here is to group the ETs together into two sets. All ETs in a given set transmit at the same center frequency. The two transmission frequencies corresponding to the two groups are only slightly separated (the complete spectrum of an ET spans only a few KHz). We describe next how to classify the ETs into separate groups using phase mismatch, such that their cumulative spectrum spread is still contained within the bandwidth of the energy harvesting (EH) circuit of the sensor node.

1) Optimal Phase Mismatch: We first perform a set of experiments to determine how much of the phase mismatch between two ETs is actually harmful. If the ETs are not completely π radians separated in phase, then some of them may even be allowed to transmit together. The resultant increase in the raw emitted power in these cases compensates for the loss owing to the slight mismatch. Fig. 2(a) shows the effect of phase difference $\Delta\phi$ between two energy transmitters on the received signal power at 433 MHz and 915 MHz. The experimental setup is the same as in Fig. 1(b). Here, the phase difference is varied from $[0, \pi]$ radians. A phase difference of 0 or 2π for the received signal (the emitted signals being in-phase), corresponds to a linear distance of one wavelength between the two transmitters. Thus, depending upon the actual distance L between the ET x and receiver node, we represent $\phi_x = (L/\lambda) \cdot 2\pi$. Here, λ is the wavelength of the transmitted radiation. From Fig. 2(a), we observe that for small phase difference, i.e., for $\Delta\phi \leq (\pi/2)$, the resultant signal signal strength is not significantly lowered (i.e., the fall is only about 1–2 dBm). This determines the optimal phase separation that is an important parameter in the protocol level design. Accordingly, all those ETs that are separated by $\Delta\phi \leq (\pi/2)$ can be grouped under one category (and center its transmissions at frequency f_1, say). Similarly, ETs that are separated by $(\pi/2) \leq \Delta\phi \leq \pi$ fall in the second category (and use frequency f_2 as the center transmission). We call this method as the *two-tone* energy transfer.

2) Optimal Distance Separation: In Fig. 2(b), using the experimental results and the relationship between the phase and distance, all the ETs separated by a multiple of the wavelength from each other, i.e., $L = m\lambda$, $m = 1, 2, \ldots$ can transmit on f_1, while the others separated by $L = (m + 1/2)\lambda$ can transmit on frequency f_2. As there are two active transmission tones present concurrently during transmission, each of these are separated in the frequency domain, one on each side of the center response point of the harvesting circuit. Both these tones must be completely encompassed by the response of the harvesting circuit at the receiver side.

We can potentially group the ETs into more than two categories. However, it can be observed from Fig. 2(a) that increasing the number of groups, results in a smaller phase difference between ETs. This results in insignificant constructive effect (i.e., about 2 dBm) on the received signal power. For example, if three groups of ETs are to be employed, the decision region will be $\lambda/3$ and the received signal power is only slightly affected by $\pi/3$ phase mismatch. On the other hand, increasing the number of groups will increase the chance of more destructive

interference, especially for EH circuit with narrow bandwidths. More groups also increase hardware complexity and energy transfer delay, which are described later in Section V-A. Also, it noteworthy that the 99% occupied bandwidth of the currently used Powercaster ET is relatively small, approximately 63 kHz, thereby allowing us to accommodate the entire transmission spectrum of the ET within the 900 MHz frequency response curve of the EH circuit we designed in [1].

C. Energy Charging Time

As ETs transmit at comparatively higher energy levels in the same band (34 dBm using Powercaster transmitter [2] in our testbed, compared to -20 dBm for the Mica2), a much larger area is rendered unusable for data communication. For example in Fig. 1(a), even if $S2$ is situated at a considerable distance away from ET x, it will still fall within its interference band (shown by the area with dotted lines) and unable to receive data. Thus, the sensor nodes need to balance between the communication and charging times so that (i) prevent extended durations of communication outage and (ii) allocate charging durations per energy request based on the traffic load to adaptively sync the energy harvesting and consumption demands. Accordingly, the effective duration for which charging is allowed plays an important role in the performance and design of a new MAC protocol.

D. Requesting and Granting Energy

In a network with multiple ETs, the process of requesting energy by the sensor nodes and granting energy by the ETs require a timely coordination and cooperation. The MAC protocol must decide (i) when and how a sensor should actually request energy from neighboring ETs, (ii) when the ETs should start transferring energy, (iii) how ETs know about suitable charging duration and the choice of frequency need to be addressed.

E. Data vs. Energy Channel Access

At the time the sensor node needs energy, the residual energy of the requesting node is very low. Thus, the medium access control should give higher priority to energy requests over data in the channel access. This design issue is not incorporated into the classical MAC protocols, and needs to be carefully considered in the design of RF-MAC. Note that issues such as when, how long, and how frequently ETs access to the channel are determined by charging time and energy requesting and granting process.

IV. RF-MAC Protocol Overview

At a high level, the medium access control mechanism in the RF-MAC protocol is organized into three components—(i) *joint ET-spectrum selection*, (ii) *adaptive charging threshold selection*, and (iii) *energy-aware access priority*. We now give an overview the RF-MAC protocol, and in the next section, we describe its detailed operation.

- *Joint ET-spectrum Selection*: In this phase, the energy requesting node issues its request for energy (RFE) packet. The ETs that receive this request independently separate themselves into two groups slightly separated in the center frequency, but still contained within the transmission band. The ETs use the signal strength of the RFE to estimate their (rough) individual distances to the requesting sensor to identify in which group they belong (see Section III-B) and reply with a cleared for energy (CFE) pulse. Depending upon which group of ETs supplies higher level of energy, the requesting sensor solves an optimization framework to assign center frequencies to these two groups. This technique incorporates consideration of the (i) the destructive effect (i.e., energy cancellation) of concurrent energy transmissions, and (ii) the spectrum response of the EH circuit, which is an important physical layer characteristic.
- *Adaptive Charging Threshold*: In this phase, the energy requesting sensor node determines its upper charging level threshold and the charging duration, based on its local network conditions. This threshold is unique for a given node, and is derived from the ratio of its own data communication activity to that observed in its neighborhood. The charging duration determines how long the data communication should be disrupted.
- *Energy-Aware Access Priority*: This phase has two main functionalities. First, it gives higher priority to the energy request packets than the data packets for accessing the channel by defining different durations for the slot time for data and energy access. The slot time is the fundamental time unit for channel access and exponential back off calculations in CSMA/CA. Second, it adapts the sensor's back-off duration based on its residual energy. Thus, the sensor with higher residual energy has a higher access priority for data communication.

A. Example Operation of RF-MAC

As an example, in Fig. 3, three sensors $S1$, $S2$, and $S3$ have residual voltages of 2.6, 2.3, and 3.0 V, respectively. Since the voltage of $S2$ has reached a pre-set threshold, 2.3 V, this node sends out the RFE packet requesting for immediate charging. RF-MAC, through the *access priority* mechanism (Section V-C), ensures that $S2$ wins the channel access for energy transfer earlier than $S1$ and $S3$ that have data packets to deliver. At this time, $S1$ and $S3$ are forced to freeze their backoff timers and get into charging mode, as data communication is infeasible. Once RFE packet is received by the ETs, they reply back with the CFE, which is a short energy pulse.

Node $S2$ identifies the two sets of ETs by measuring the received power of CFEs and determines their associative optimal energy transfer frequencies (Section V-A). How much should $S2$ charge depends upon the *adaptive charging threshold selection* (Section V-B). The node $S2$ then sends out an ACK packet to the ETs in which it includes the optimal frequencies as well as the charging duration. Finally, when nodes $S1$ and $S3$ compete for data transfer, *access priority* ensures their respective backoff windows are a function of the residual energy (Section V-C). Assuming that $S1$ has higher residual energy, it will likely get the data communication opportunity

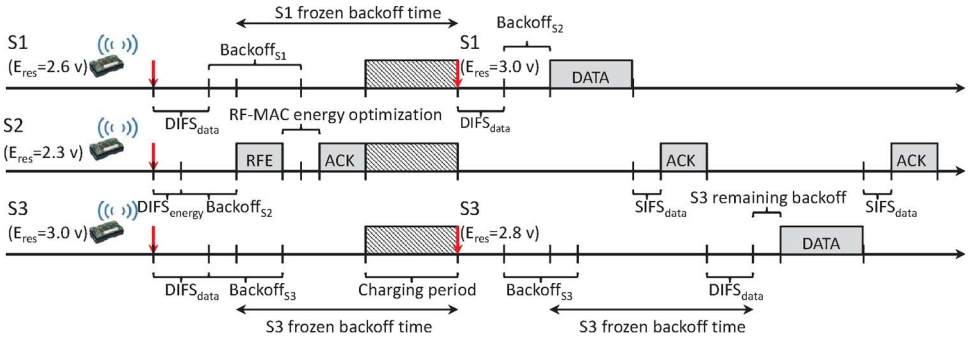

Fig. 3. Example scenario for overview of RF-MAC protocol with three RF energy harvesting sensor nodes.

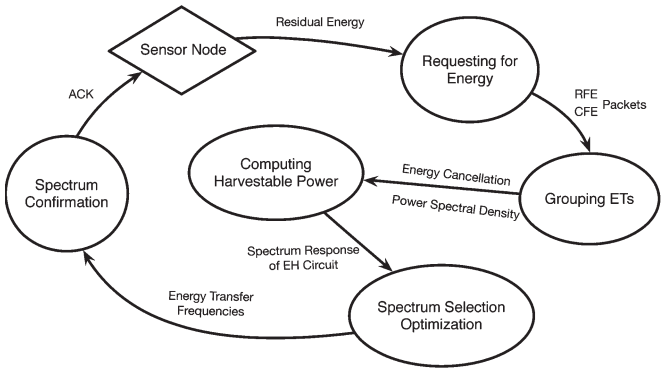

Fig. 4. Five stages of joint ET-spectrum selection component in RF-MAC protocol.

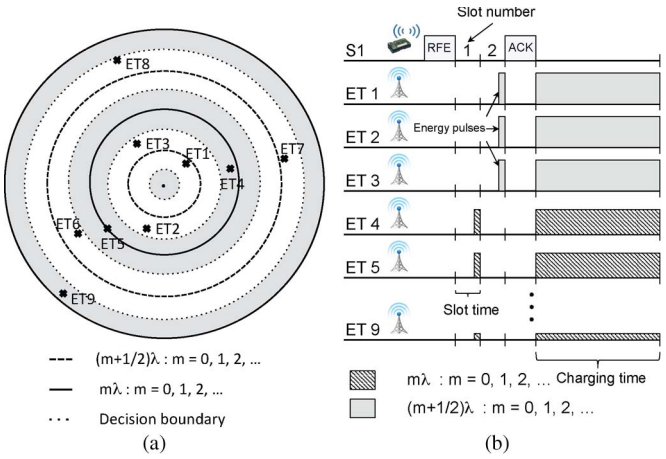

Fig. 5. Grouping and selection of ETs based on the destructive interference of energy waves (a), the timing diagram for requesting and granting energy in the RF-MAC protocol (b).

first, followed by $S3$. The latter freezes the countdown timer in this duration, and resumes the remaining countdown as soon as the channel is next available.

The details of the above three phases and the complete RF-MAC protocol description is given in the next section.

V. Detailed RF-MAC Protocol Description

A. Joint ET-Spectrum Selection

As shown in Fig. 4, the specific stages considered during the joint ET-spectrum selection are (i) requesting for energy, (ii) grouping ETs based on destructive interference, (iii) computing harvestable power, (iv) spectrum selection optimization, and (v) spectrum confirmation.

1) Requesting for Energy: The sensor node broadcasts the RFE packet, requesting for energy, when its voltage falls below a pre-set threshold ($\sim$2.3 V, as minimum operating voltage of the Mica2 is 1.8 V). The RFE contains the requesting sensor node's ID, transmitted at constant signal strength. This RFE can be sent when the channel is free, i.e., when there is no ongoing data transfer or energy charging operation and the channel lies idle for the DIFS_{energy} duration (calculation of this channel sensing duration is described later in Section V-C). The ETs that receive this packet estimate roughly their distances from the node, based upon the received signal strength (RSS). In the following, we define that the distance measurement only needs to determine a *band* in which the ET lies, and not its exact location.

2) Grouping ETs Based on Destructive Interference: Recall from Section III, the distance between the ET and the sensor node directly results in a phase difference of the incoming wireless signals at the node. The ETs that identify themselves to lie in the band $[m\lambda - (\lambda/4), m\lambda + (\lambda/4)]$, are grouped together, where $m = \{1, 2, \ldots\}$. We call this as `Group I`. Similarly, the other ETs in the range $[(m + 1/2)\lambda - (\lambda/4), (m + 1/2)\lambda + (\lambda/4)]$ fall in the second group, called `Group II`. Thus, on receiving the RFE, each ET knows which concentric band it lies in centered around the requesting node, and the group in which it belongs. Fig. 5(a) shows a sample scenario. The shaded region depicts the ETs 4 and 5 that lie in the band of λ, i.e., in `Group I`. This region extends up to $\lambda/4$ on either side of the central bold line that lies at an exact distance of λ with the requesting node placed at the center. Since we do not precisely require the ET to calculate the distance from the requesting node, but only need to determine if it lies within a concentric band-region, our approach is more robust to RSS fluctuations. Of course, using a dedicated localization scheme or GPS hardware considerably eases this constraint, though adding to the implementation cost and power requirement.

The ETs that hear the RFE reply back with a single and constant energy pulse. Each concentric band has the choice of one of two time slots in which this pulse may be emitted, beginning from the instant of completion of the RFE, as shown in Fig. 5(b). Referring again to the band structure in Fig. 5(a), the first slot is allocated for CFE pulses sent by energy transmitter of `Group I` (note: all `Group I` bands are shown shaded). Similarly, CFE pulses from energy transmitters of Group II are

sent during the second slot, i.e., ETs 1, 2 and 3 collectively lie in the second concentric (`Group II`) band and simultaneously transmit their pulses in the second slot.

3) Computing Harvestable Power: The node that sent the initial RFE estimates the total energy that it will receive based on the signal strength of the CFE pulses in the slot number in which they were received. This arrangement of using the pulses allows the ETs to be simple in design, and removes the concern of collisions. Unlike classical data communication, it is not important for the node to know *which* ET will transmit energy. Rather, its energy calculations are based on *how much* energy is contributed by the two groups of ETs separately. We define this cumulative energy as $E_{RX}^{Group\ I}$ and $E_{RX}^{Group\ II}$, respectively, which are calculated by the RFE issuing node from the received pulses. Each slot time is 10 μs in our work, allowing a very fast response time. The purpose of differentiating the energy contribution from the two groups is useful in the next stage, where an optimization function returns the center frequencies of the ETs.

4) Spectrum Selection Optimization: Let `Group I` ETs be centered at frequency f_1, and `Group II` ETs be centered at frequency f_2 so that they can concurrently transfer energy without destructively affecting each other. How to select these frequencies f_1 and f_2 is explained next, which takes into account two important physical layer characteristics of the energy transfer. The first is the spectrum response of the energy harvesting circuit that is connected to the sensor nodes, shown by the envelope $H(f)$ in the frequency domain in Fig. 2(b). The physical bandwidth of energy harvesting circuit is denoted by BW_{EH}. The power spectral density (PSD) of the two groups of ETs is the other concern, represented by $S_1(f)$ and $S_2(f)$, respectively, for `Group I` and `Group II`. The sensor node observes these shapes from the incoming pulses from the ETs. Thus, the bandwidth 2ε of the transmission spectrum (centered at f_1 and f_2) must be selected in such a way there is a minimum overlap between their individual spectra, and yet contained within the envelope of $H(f)$. We use the following optimization if the transmission spectrum of the ETs occupies a bandwidth of 2ε.

The aim of the optimization formulation is to maximize the energy transfer $E_{RX}^{Max} = E_{RX}^{Group\ I} + E_{RX}^{Group\ II}$, which at a given frequency point is the product of the power spectral density and the circuit frequency response. Thus, the useful components that need to be maximized are the first two terms of (2), which give the constructive energy contribution of the ETs of the two groups

$$\begin{aligned} &Given:\ S_1(f), S_2(f), BW_{EH}, H(f) \\ &To\ find:\ f_1, f_2, \gamma \\ &To\ Maximize: \end{aligned} \tag{1}$$

$$E_{RX}^{Max} = \int_{f_1-\varepsilon}^{f_1+\varepsilon} S_1(f)H(f)\mathrm{d}f + \int_{f_2-\varepsilon}^{f_2+\varepsilon} S_2(f)H(f)\mathrm{d}f - \underbrace{\left(\int_{f_2-\varepsilon}^{\gamma} S_2(f)H(f)\mathrm{d}f + \int_{\gamma}^{f_1+\varepsilon} S_1(f)H(f)\mathrm{d}f\right)}_{\text{destructive interference}} \tag{2}$$

$$Subject\ to: \quad |f_2 - f_1| < BW_{EH} \tag{3}$$

$$\left.\frac{d\left(S_1(f)H(f)\right)}{\mathrm{d}f}\right|_{f=\gamma} < 0 \tag{4}$$

$$\left.\frac{d\left(S_2(f)H(f)\right)}{\mathrm{d}f}\right|_{f=\gamma} > 0. \tag{5}$$

The first constraint is to ensure that both frequency groups are contained within the bandwidth of the energy harvesting circuit. The constraints (4) and (5) ensure that the spectrum shapes of the `Group I` and `Group II` ETs does not overlap completely. We assign f_1 to the left of f_2 on the frequency scale (see Fig. 2(b)). At the point of the intersection of the PSD curves $S_1(f)$ and $S_2(f)$, which we call the *cross-over* point γ, the slope of the curves must be positive and negative, respectively. This is calculated by differentiating the respective PSD plots at γ, to ensure that one of them increases (positive slope) while the other falls (negative slope).

A problem is said to have an optimal substructure if an optimal solution can be constructed efficiently from optimal solutions to its sub-problems. We claim that our proposed optimization also exhibits the optimal substructure property. The proof is included in the Appendix.

5) Spectrum Confirmation: With the resulting dual-frequency wireless energy transfer, both groups of ETs can be simultaneously active. The final part of this stage involves letting the ETs know that they are cleared for energy transmission through an Acknowledgement (ACK) packet. This packet provides the ETs the center point for the frequencies f_1 and f_2, according to the results of optimization. The ETs know which group they belong to internally, based on the RSS-based band structure shown in Fig. 5(a). Additionally, the ACK carries an estimated charging time T based on a target voltage level of the capacitor (calculated in Section V-B). This upper limit on the charging voltage is decided by the node's relative activity in the neighborhood.

After a short SIFS wait period following the ACK (using shorter slot times, for energy, compared to those used for data communication), the ETs begin their transmission. In case of loss of the RFE due to packet collision or bad channel conditions, the contention windows are re-set to the minimum width, thereby initiating an immediate subsequent retry. The idea here is that (i) time is critical when a node has extremely low voltage and (ii) nodes will require energy recharging opportunities much less than the data communication opportunities [18]. Hence, the number of energy request packets will be less than data packets and there will not be frequent collision related losses of the RFE arising from the shorter contention window.

From our preliminary experimental results, we recall that increasing the number of groups to more than two has a negligible constructive effect on the received signal power (see Section III-B2). In addition to this, we find that introducing an additional frequency group, say `Group III` with PSD $S_3(f)$, increases the chance of more destructive interference, and in the optimization formula the destructive interference term increases from 2 terms (all overlapping areas of $S_1(f)$ and $S_2(f)$) to at least 4 terms (all overlapping areas of $S_1(f)$, $S_2(f)$, $S_3(f)$). Furthermore, as the number of groups increases the number of slot times for CFE pulses and computing the harvestable power also increases. Clearly, this results in additional

delay in granting energy to the sensor nodes. Finally, more than two groups of energy transmitters mean tighter location detection requirement and hence most likely more expensive hardware.

B. Adaptive Charging Threshold

As our energy transfer is in-band, each node needs to decide the charging time that may possibly result in a reduced level of energy replenishment. Our proposed method defines this upper charging level based on the level of participation in data communication activity for that node with respect to its neighbors. Each node maintains a moving average of the time spent by itself in transmitting and receiving data packets to the total time the channel is used or sensed as *busy*. Many nodes, hence, will never charge to their maximum capacity, and thereby, they sacrifice their charging opportunity for the larger good of the network performance. The node's *importance index* (IDX) is shown in (6), where Tx represents the number of data packets that originate from it and Rx denotes the number of packets destined for the node. Data transfer activity, overhead by the node, that neither originate nor end at it are expressed through *Channel busy time*. The upper charging voltage $V_{\max}^{threshold}$ is calculated from (7)

$$IDX = \frac{Tx + Rx}{Tx + Rx + Channel\ busy\ time} \tag{6}$$

$$V_{\max}^{threshold} = IDX \times (V_{\max} - V_{\min}) + V_{\min}. \tag{7}$$

The charging time T that the node includes in the ACK is calculated as follows, using the standard definitions of energy stored in the capacitor, (7) and the trigger voltage $V_{\min}^{threshold}$ under which the RFE is set out by the node

$$T = \frac{1}{2}C\left\{\left(V_{\max}^{threshold}\right)^2 - \left(V_{\min}^{threshold}\right)^2\right)\right\}\frac{2Slot_{energy}}{E_{RX}^{Max}}. \tag{8}$$

Here, the received energy during the CFE pulses is obtained from two successive time slots, each of duration $Slot_{energy}$.

C. Energy-Aware Access Priority

This channel access determining feature of the RF-MAC manifests in two ways: The first is prioritizing between energy transfer and data communication, and secondly, identifying which nodes within the network should send out the data packets first by winning the channel.

1) Energy Transfer Prioritization: The residual energy of the requesting node is below a threshold $V_{\min}^{threshold}$ when it sends the RFE, and hence, it should have higher priority in channel access. This is ensured by separately defining the DIFS duration for energy and data. Consequently, the specially formulated energy request DIFS duration (DIFS_{energy}) is shorter than DIFS for data exchange (DIFS_{data}), achieved by assigning a shorter slot time for energy request, while data exchange is provisioned with a longer slot time. Hence, we use the slot time of 10 μs for energy request and 20 μs for data communication as defined in the 802.11 standard [3]. Since DIFS is defined as $\mathrm{SIFS} + 2\mathrm{Slot\ time}_{energy}$, we derive 25 μs for DIFS_{energy} and 50 μs for DIFS_{data}. With the shorter DIFS duration and slot time, RF-MAC prioritizes the energy request over data exchange. Note that DIFS and SIFS are defined acronyms in 802.11 standard [3]. The time calculations for the protocol are given in Table I.

TABLE I
PARAMETERS USED IN RF-MAC

Parameter	Value
slot time	10μs (energy), 20μs (data)
CW_{min}	32
CW_{max}	1024
DIFS_{energy}	SIFS_{energy} + 2Slot time_{energy} = 25 μs
DIFS_{data}	SIFS_{data} + 2Slot time_{data} = 50 μs
SIFS	5 μs (energy), 10 μs (data)

2) Data Transfer Prioritization: In the data exchange phase, the sensor contends for a channel using the CSMA/CA mechanism defined in 802.11 [3], i.e., it senses the channel for the DIFS duration before attempting a transmission. Consequently, sensors with higher energy harvesting rate, owing to their position or channel characteristics between the ETs and themselves, will have shorter charging durations. They will be able to participate timely for data communication, without interruptions and packet drops for frequent replenishment of energy, all of which contribute to the energy usage. We assign sensors with higher residual energy level a correspondingly higher priority to transmit. [11] proves analytically that this method results in an asymptotically optimal network lifetime. We design RF-MAC in such a way that the sensor's backoff duration is influenced by its residual energy, i.e., the node with higher residual energy experiences a shorter backoff duration than the node with lower residual energy. An example of the adaptive backoff mechanism for data exchange is described in (9), as shown at the bottom of the page. The contention window for data exchange (CW_{data}) is randomly selected from the range between the minimum CW and node's current CW, $[CW_{\min}, CW_{current}]$. We set the contention window of 32 for $CW_{\min}$ in this work. Further, (9) shows how the effective slot time is a scaled value based on the residual energy. The capacitor voltage is used for scaling, where it is limited at the high end by the rated voltage of the capacitor $V_{\max}$ (note this is different from the upper charging threshold in (9), current voltage $V_{current}$, and the $V_{\min}^{threshold}$ that signals a critical point if the sensor needs to be kept in operation. (See equation at bottom of the page).

$$Backoff = \underbrace{DIFS_{data} + CW_{data} \times \left\{Slot_{energy} + \frac{(V_{\max} - V_{current})(Slot_{data} - Slot_{energy})}{V_{\max} - V_{\min}^{threshold}}\right\}}_{adaptive\ slot\ time} \tag{9}$$

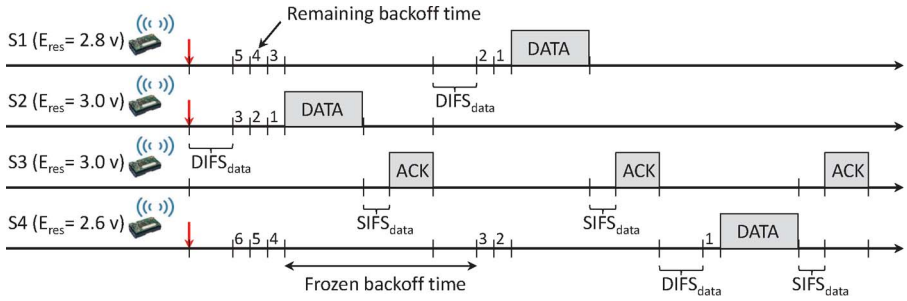

Fig. 6. Energy-aware data exchange process in RF-MAC protocol with three transmitter nodes S_1, S_2, and S_4 and the receiver node S_3.

The overall process of data exchange is explained using Fig. 6. Sensors $S1$, $S2$, and $S4$ all have packets to transmit to sensor $S3$ at the start (indicated by the arrow on the time axis). They each sense the channel for DIFS_{data}. Intuitively from (9), sensor $S2$ with the residual energy of 3.0 V, should experience the shortest backup duration, as opposed to $S1$ and $S4$. However, this does not imply that the nodes with higher residual energy will *always* have a shorter back off duration, as the random selection of the backoff slots within the window does contribute to the overall backoff time. This selection of the window $[CW_{\min}, CW_{current}]$ is independent of node's residual energy.

VI. Simulation Results

In this section, we evaluate the performance of our RF-MAC protocol using the ns-2 network simulator, with experimental results presented in the next section. We demonstrate the performance improvement with respect to the following metrics: (i) number of energy transmitters, (ii) number of data flows, (iii) numbers of nodes, and (iv) packet size. The primary performance metrics are the average network throughput and the average harvested energy. In particular, the first metric shows the average per-node throughput of the sensor network, and the second metric gives the average energy harvested per-node that is found by recording and averaging the harvested power by nodes during the simulation.

The simulation parameters are set as follows. The EH circuit parameters are from [1]. We model the ETs on the Powercaster transmitter [2], which radiates continuous waves at 3 W. The operational characteristics of the sensor, such as energy spent on transmission, reception, idle listening, channel bandwidth, etc. are from Mica2 specifications [10]. Unless specifically stated, 250 sensor nodes and 100 ETs are deployed uniformly at random in 50×50 m^2 grid. Traffic loads are generated by constant bit rate (CBR) flows. Nodes have a full buffer and all data packets are 50 bytes in size. The sender/receiver pairs are chosen randomly, and the intermediate relaying nodes do not aggregate or compress data. Additional parameters used in the simulation are presented in Table I.

We compare three different protocols: 1) RF-MAC-opt, 2) RF-MAC-no-opt, and 3) modified unslotted CSMA. RF-MAC-opt is the full-featured RF-MAC, including the joint spectrum-ET selection, adaptive charging threshold, and energy-aware channel access priority mechanisms, as discussed in Section IV. The RF-MAC without the optimization (named RF-MAC-no-opt) has all components of RF-MAC other than joint spectrum-ET selection component. In particular, it does not assign different frequencies to the ETs and makes no attempt to identify and classify ETs based on their phase mismatch. We evaluate the RF-MAC-opt against RF-MAC-no-opt in order to investigate the effectiveness of the joint spectrum-ET selection feature incorporated in our RF-MAC protocol, especially in avoiding energy interference and improving the network performance. Finally, the modified CSMA is adapted from [4], which provides the baseline for our performance evaluations. To have a fair baseline comparison, the modified CSMA (in which each sensor node may issue the RFEs and receive the CFEs) is compared against both RF-MAC-opt and RF-MAC-no-opt. In the modified CSMA, there is no attempt made to calculate the optimal charging time, and it has none of the features of the RF-MAC protocol. Once an RFE is sent out, the node charges to its maximum capacity and does not take into consideration the impact on data traffic, energy cancellation, and the residual level of the sensor nodes. Data points in each graph represent the mean of twenty scenarios and the corresponding 95% confidence intervals are plotted as error bars in the figures.

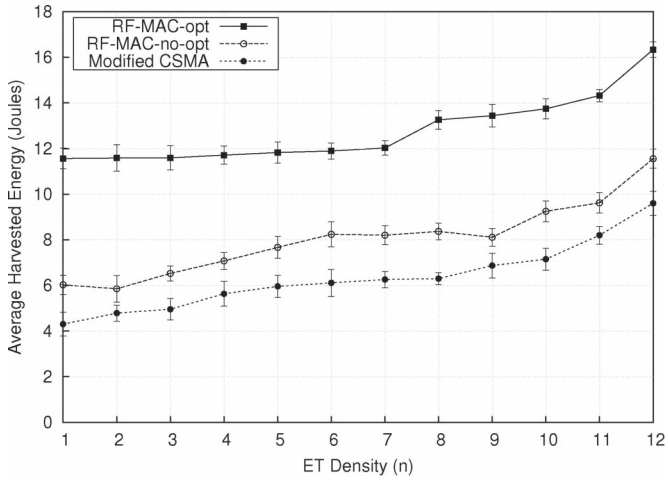

Fig. 7. Effect of the number of ETs on the average harvested energy.

A. Impact of the Number of ETs

In the first set of experiments, we investigate the effect of the number of ETs for different MAC protocols. Fig. 7 shows the effect of the ET density on the average harvested energy of two RF-MAC variants. The ET density, defined as the average number of ETs located within the radio range of a sensor node,

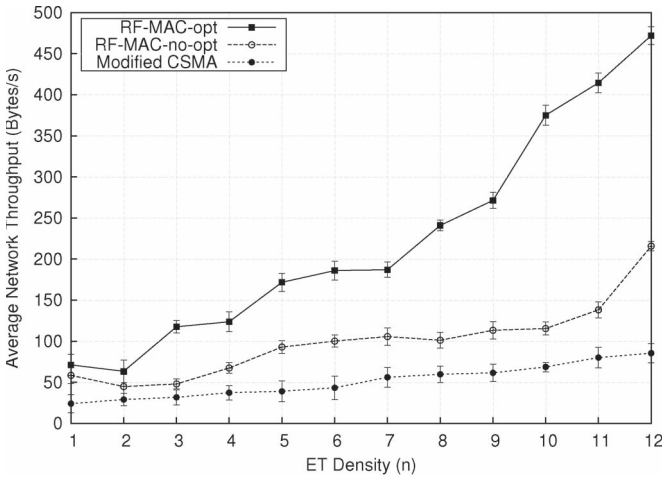

Fig. 8. Effect of the number of ETs on the average network throughput.

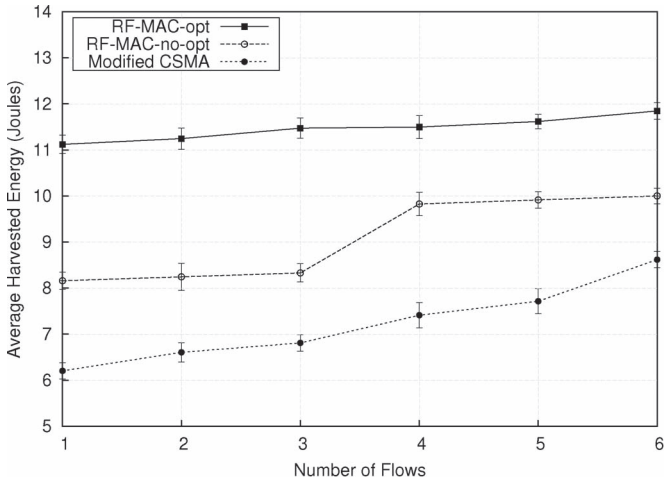

Fig. 9. Effect of multiple flows on the average harvested energy.

varies from 1 to 12. It is clear that both RF-MAC variants dominate over the modified CSMA. As shown in Fig. 7, RF-MAC-opt delivers monotonically increasing average harvested energy with increasing the number of ET density. The benefit of frequency optimization greatly improves the performance as it maximizes the energy transfer by separating two transmission spectrum and ensuring the highest level of energy delivery. Without this optimization, ETs enter the charging process and do not take into account the possibility of destructive interference, resulting in sub-optimal energy transfer.

The average network throughput is shown in Fig. 8 and the trend is observed to be very similar to the average harvested energy plot. Both variants of RF-MAC yield higher average network throughput as ET density increases. However, the throughput of RF-MAC-opt is significantly higher that RF-MAC-no-opt, with a 62% increase on average. Both the average harvested energy and average network throughput of modified CSMA are the lowest among protocols under study. This is because modified CSMA does not have the adaptive charging features included in the RF-MAC protocol. In this case, RF-MAC-opt yields over 100% and 300% more than the modified CSMA in terms of the average harvested energy and average throughput, respectively.

B. Impact of Multiple Flows

The effect of multiple simultaneous flows in the sensor network is investigated next, with random selection of source and destination nodes, while the number of flows is varied from 1 to 6. Again, we observe the behavior of RF-MAC on two energy and throughput metrics, when nodes experience different levels of channel usage and traffic loads. Fig. 9 shows a smooth and monotonic increase in the average harvested energy of RF-MAC-opt as the number of flows increases. Even though the RF-MAC-no-opt exhibits a similar pattern, the increase is not as smooth as one with the frequency optimization. Evidently, the amount of average harvested energy yield could be almost 150% less than RF-MAC-opt. Fig. 10 depicts the average network throughput of RF-MAC with various numbers of data flows. Interestingly, the average network throughput of both RF-MAC variants gracefully drops as the number of

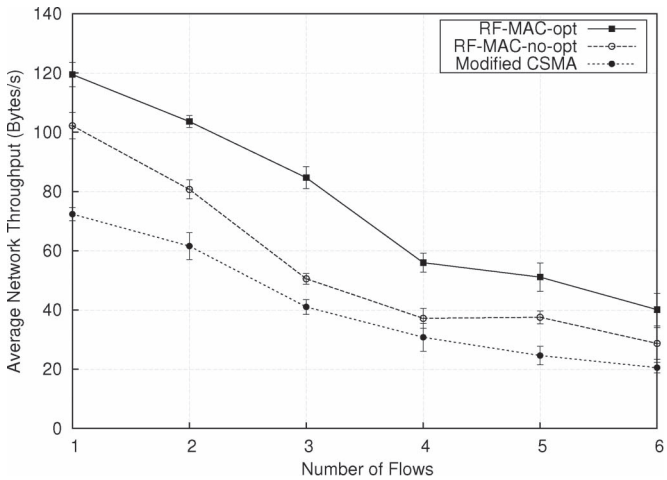

Fig. 10. Effect of multiple flows on the average network throughput.

data flow increases. This reduction in the throughput is a result of more nodes sending out RFEs as they deplete their energy faster with increasing number of data flows. Consequently, the network spends more time in the charging state and less time spent in the data exchange state. However, RF-MAC-opt yields higher average network throughput, approximately 20% more in this case. Again, both variants of RF-MAC largely outperform the modified CSMA. Especially, RF-MAC-opt yields approximately 112% increase in terms of throughput.

C. Impact of the Number of Sensor Nodes

We investigate how RF-MAC protocol behaves when the number of sensor nodes in the topology changes. We randomly deploy various numbers of sensor nodes in the topology, ranging from 60 to 240. The average harvested energy is shown in Fig. 11, wherein the performance of RF-MAC-opt smoothly drops and tends to stabilize when 120 sensor nodes or more are present. On the other hand, RF-MAC-no-opt yields a similar pattern to the modified CSMA, a rather constant average harvested energy with fluctuations around the mean trend. Again, RF-MAC-opt offers higher average harvested energy when compared to RF-MAC-no-opt. Fig. 12 depicts the average network throughput of RF-MAC with different

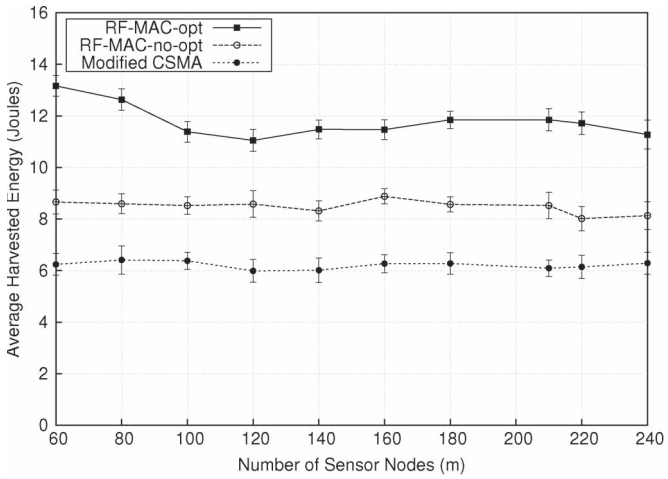

Fig. 11. Effect of the number of nodes on the average harvested energy.

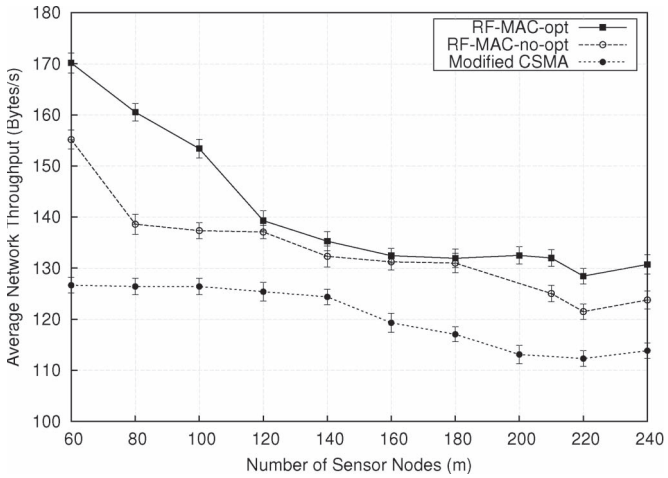

Fig. 12. Effect of the number of nodes on the average network throughput.

numbers of sensor nodes. Similar to the earlier case with the average harvested energy, both RF-MAC variants experience the reduction in average network throughput even RF-MAC-opt displays marginally higher throughput. Moreover, the modified CSMA performs significantly lower than RF-MAC-opt and RF-MAC-no-opt in both harvested energy and network throughput.

D. Impact of Packet Size

The packet size is varied from 30 to 90 bytes with an increment of 20 bytes, while other parameters are kept to their default settings. The impact of packet size on the average harvested energy of RF-MAC is shown in Fig. 13. It is clear that the average harvested energy of RF-MAC-opt is monotonically increasing with an increasing packet size, and offers up to 25% gain over RF-MAC-no-opt at the packet size of 90 bytes. On the other hand, the average harvested energy of RF-MAC-no-opt tends to stabilize for packet sizes larger than 50 bytes. The average network throughput of RF-MAC is shown in Fig. 14. Both RF-MAC variants offer an increase in average network throughput with increasing packet size. Again, the RF-MAC-opt outperforms, in terms of the average network throughput, its non-optimized variant and the modified CSMA throughout the study range.

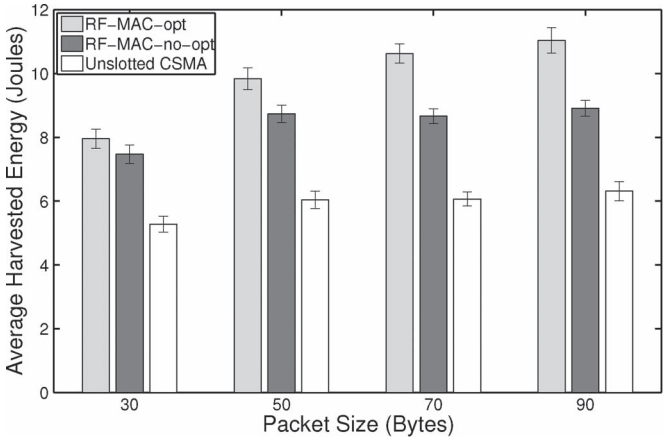

Fig. 13. Effect of the packet size on the average harvested energy.

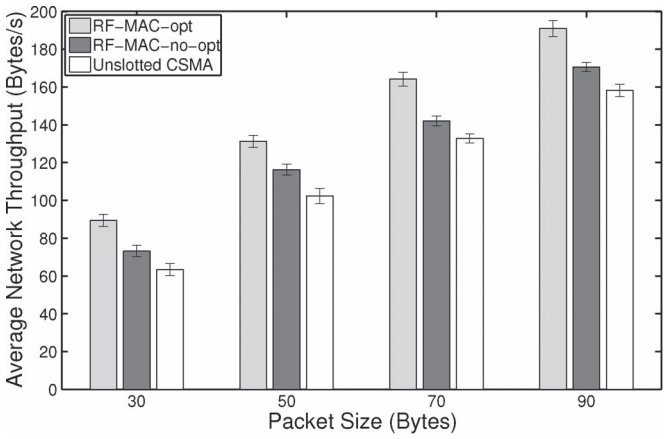

Fig. 14. Effect of the packet size on the average network throughput.

VII. Experimental Study

Our testbed consists of 4 parts, signal generators (Agilent N5181 MXG RF signal generators), RF switches, RF amplifiers of 3 W EIRP (to emulate two ETs), and three wireless sensors. We implemented the RF-MAC protocol in Mica2 motes equipped with Chipcon CC1000 radios and connected to our in-house fabricated RF energy harvester [1] operating at 915 MHz. The sender motes are programmed to continuously transmit 30 Byte packets to the sink. We use the following setup to build the two ETs for the transmission of wireless RF power, whose schematic is shown in Fig. 15. The signal generators produce two energy waves with bandwidth 63 kHz (similar to Powercaster transmitter [2]) that are slightly shifted, corresponding to the frequencies f_1 and f_2 obtained in frequency assignment optimization earlier. These frequencies for our energy harvesting setup are found as $f_1 = 915$ MHz and $f_2 = 916$ MHz. This assures that transmission of the ETs and the sensor motes are in-band and mechanisms such as data vs. energy channel access can be verified correctly through the experiments. The ET controller sends appropriate interrupt signal to the RF switch upon receiving the ACK packet from the energy requesting node. We also programmed Mica2 mote to function as an ET controller by using three interrupt pins of the mote's expansion connector based on the MPR/MIB User's Manual [10]. Specifically, INT0 is used to disable and enable the RF switch, INT1 is used

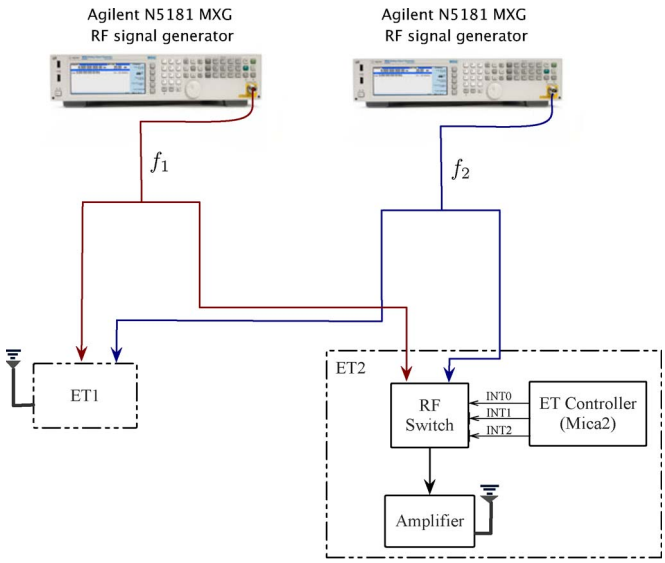

Fig. 15. Schematic of our experimental setup for transmission of wireless RF power.

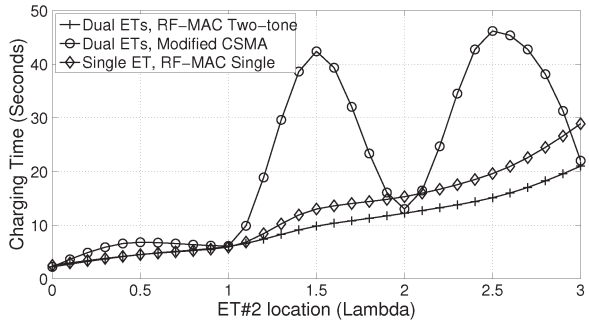

Fig. 16. Effect of ET2 position on the average harvested energy.

to select output frequency f_1, and INT2 is used for selecting output frequency f_2. Accordingly, the RF switch passes the selected input signal to the RF amplifier which then transmits with output power 3 W EIRP. Note that in the testbed both ET1 and ET2 have the same configurations, with the interior working of one of them expanded for brevity.

In order to verify the benefit of RF-MAC variants (two-tone and single-tone energy transfer) over the modified CSMA, the RF harvester is fixed at the location 0λ, ET1 is fixed in location 3λ away from the harvester, while the location of ET2 is varied between location 0λ to 3λ. We evaluate the testbed under three different scenarios as follows:

- Both ET1 and ET2 adopt RF-MAC with two-tone energy transfer (f_1 at 915 MHz and f_2 at 916 MHz).
- Both ET1 and ET2 adopt RF-MAC with single-tone energy transfer (only one group is transmitted on f_1 at 915 MHz).
- Both ET1 and ET2 adopt the modified CSMA that does not employ frequency assignment optimization.

The average charging time and the network throughput of the testbed under various MAC protocols are shown in Figs. 16 and 17. Each point in the experimental results represents an average of ten independent experiments for 95% confidence interval with 5% precision. It is clear that the RF-MAC with

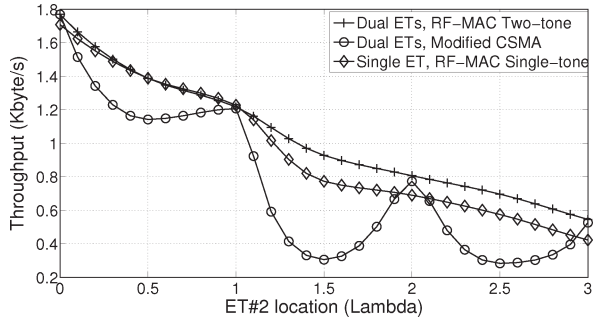

Fig. 17. Effect of ET2 position on the average network throughput.

two-tone energy transfer not only yields the highest average network throughput and the lowest charging time but also it experiences minimal fluctuations. On the other hand, the modified CSMA gives the highest charging time and the lowest network throughput when ET2 is not located at the position that results in in-phase combination of energy waves at the harvester. The RF-MAC protocol prevents destructive effects by out-of-phase combination of energy waves, and consequently achieves higher average network throughput. Moreover, the RF-MAC with two-tone energy transfer provides additional improvements in the receiving power when compared to single-tone energy transfer since both ET1 and ET2 can operate simultaneously. There exists a region where destructive effect is less pronounced, i.e., when ET2 is varied from location 0λ to 1λ. This is because the power provided by ET2 is much higher when compared to the one provided by ET1. ET2 power and phase simply dominates the behavioral outcome. However, it can be observed that the destructive effect is more pronounced when ETs are distanced equally, i.e. ET2 at 2.5λ or 3.5λ when ET1 is at 3λ.

VIII. Conclusions

In this paper, we proposed the RF-MAC protocol that specifically addresses the problems of the joint selection of energy transmitters and their frequencies based on the collective impact on charging time and energy interference, setting the maximum energy charging threshold, requesting and granting energy, and energy-aware access priority. The grouping of the ETs into two sets with varying transmission frequencies, and the minimal control overhead are both geared to keep the hardware requirements simple, and the protocol easier to implement. Our protocol delves on the important issue of how to determine the energy vs. data communication tradeoff, especially as one occurs as the cost of the other. Finally, simulation and testbed results reveal that RF-MAC largely outperforms the modified CSMA in both average harvested energy and average network throughput.

Appendix
Proof of Optimality of Energy Transfer

Statement: Given the power spectral density $S_1(f)$ and $S_2(f)$, the total energy transfer (E_{RX}^{Max}) under the RF energy harvesting

circuit's frequency response $H(f)$ is maximum.

$$E_{RX}^{Max} = \underbrace{\int_{f_1-\varepsilon}^{f_1+\varepsilon} S_1(f)H(f)\mathrm{d}f}_{(1)} + \underbrace{\int_{f_2-\varepsilon}^{f_2+\varepsilon} S_2(f)H(f)\mathrm{d}f}_{(2)} - \left\{ \underbrace{\int_{f_2-\varepsilon}^{\gamma} S_2(f)H(f)\mathrm{d}f}_{(3)} + \underbrace{\int_{\gamma}^{f_1+\varepsilon} S_1(f)H(f)\mathrm{d}f}_{(4)} \right\}$$

is maximum then

$$\underbrace{\int_{f_1-\varepsilon}^{f_1+\varepsilon} S_1(f)H(f)\mathrm{d}f - \int_{f_2-\varepsilon}^{\gamma} S_2(f)H(f)\mathrm{d}f}_{X} \text{ and}$$

$$\underbrace{\int_{f_2-\varepsilon}^{f_2+\varepsilon} S_2(f)H(f)\mathrm{d}f - \int_{\gamma}^{f_1+\varepsilon} S_1(f)H(f)\mathrm{d}f}_{Y}$$

are maximum as well.

Proof: Let (1)–(3) give the area under the curve represented by X and (2)–(4), similarly, return the area of Y, then $(1)+(2)-\{(3)+(4)\}$ has the total area of $\mathrm{X}+\mathrm{Y}$. Assume we find α such that $\alpha=(1)-(3)+\epsilon$; $\epsilon>0$ then the total area $=(1)+(2)-\{(3)+(4)\}+\epsilon=X+Y+\epsilon>X+Y$. This contradicts the supposition that $(1)+(2)-\{(3)+(4)\}$ is maximum. $(1)-(4)$ can be proved in a similar fashion. ■

REFERENCES

[1] P. Nintanavongsa, U. Muncuk, D. R. Lewis, and K. R. Chowdhury, "Design optimization and implementation for RF energy harvesting circuits," *IEEE J. Emerging Sel. Topics Circuits Syst.*, vol. 2, no. 1, pp. 24–33, Mar. 2012.

[2] Powercast Corporation, Lifetime Power Evaluation and Development Kit. [Online]. Available: http://www.powercastco.com/products/development-kits/

[3] *Wireless LAN Medium Access Control (MAC) and Physical Layer (PHY) Specification*, IEEE 802.11, 1999.

[4] Z. A. Eu, H. P. Tan, and W. K. G. Seah, "Design and performance analysis of MAC schemes for wireless sensor networks powered by ambient energy harvesting," *Ad Hoc Netw.*, vol. 9, no. 3, pp. 300–323, May 2011.

[5] P. Nintanavongsa, M. Y. Naderi, and K. R. Chowdhury, "Medium access control protocol design for sensors powered by wireless energy transfer," in *Proc. IEEE INFOCOM*, Apr. 2013, pp. 150–154.

[6] J. Kim and J. W. Lee, "Energy adaptive MAC protocol for wireless sensor networks with rf energy transfer," in *Proc. IEEE ICUFN*, 2011, pp. 89–94.

[7] F. Iannello, O. Simeone, and U. Spagnolini, "Medium access control protocols for wireless sensor networks with energy harvesting," *IEEE Trans. Commun.*, vol. 60, no. 5, pp. 1381–1389, May 2012.

[8] M. K. Watfa, H. AI-Hassanieh, and S. Selman, "Multi-hop wireless energy transfer in WSNs," *IEEE Commun. Lett.*, vol. 15, no. 12, pp. 1255–1277, Dec. 2011.

[9] J. Curty, M. Declercq, C. Dehollain, and N. Joehl, *Design and Optimization of Passive UHF RFID Systems*. New York, NY, USA: Springer-Verlag, 2007.

[10] Crossbow Technology, Inc. [Online]. Available: http://www.xbow.com/

[11] Y. Chen and Q. Zhao, "An integrated approach to energy-aware medium access for wireless sensor networks," *IEEE Trans. Signal Process.*, vol. 55, no. 7, pp. 3429–3444, Jul. 2007.

[12] L. Chen, I. Demirkol, and W. Heinzelman, "Token-MAC: A fair MAC protocol for passive RFID Systems," in *Proc. IEEE GLOBECOM*, Dec. 2011, pp. 1–5.

[13] A. P. Sample, B. H. Waters, S. T. Wisdom, and J. R. Smith, "Enabling seamless wireless power delivery in dynamic environments," *Proc. IEEE*, vol. 101, no. 6, pp. 1343–1358, Jun. 2013.

[14] T. Zhu, Z. Zhong, Y. Gu, T. He, and Z.-L. Zhang, "Leakage-aware Energy Synchronization for Wireless Sensor Networks," in *Proc. 7th Intl. Conf. MobiSys*, Jun. 2009, pp. 319–332.

[15] M. Y. Naderi, S. Basagni, and K. R. Chowdhury, "Modeling the residual energy and lifetime of energy harvesting sensor nodes," in *Proc. IEEE GLOBECOM*, Dec. 2012, pp. 3394–3400.

[16] S. Basagni, M. Y. Naderi, C. Petrioli, and D. Spenza, *Mobile Ad Hoc Networking: The Cutting Edge Direction, Chapter 20: Wireless Sensor Networks with Energy Harvesting*. Hoboken, NJ, USA: Wiley, Mar. 2013, pp. 701–736.

[17] X. Fafoutis and N. Dragoni, "ODMAC: An on-demand MAC protocol for energy harvesting wireless sensor networks," in *Proc. 8th ACM Symp. PE-WASUN*, 2011, pp. 49–56.

[18] P. Nintanavongsa, R. Doost, M. Di Felice, and K. Chowdhury, "Device characterization and cross-layer protocol design for RF energy harvesting sensors," *Pervasive Mobile Comput.*, vol. 9, no. 1, pp. 120–131, Feb. 2013.

[19] M. Gorlatova, A. Wallwater, and G. Zussman, "Networking low-power energy harvesting devices: Measurements and algorithms," in *Proc. IEEE INFOCOM*, Apr. 2011, pp. 1602–1610.

M. Yousof Naderi (M'09) received the B.Sc. degree in computer engineering from Shahid Beheshti University (National University of Iran), Tehran, Iran, in 2008 and the M.Sc. degree with honors in communication and computer networks from Sharif University of Technology, Tehran, in 2010. Currently, he is pursuing the Ph.D. degree in the Electrical and Computer Engineering Department at Northeastern University, Boston, MA, USA.

His current research interests lie in the design and experimentation of novel communication protocols, algorithms, and analytical models specialized for wireless energy harvesting networks, cognitive radio networks, multimedia sensor networks, and cyber-physcial system.

Prusayon Nintanavongsa (M'12) received the B.E. degree in electrical engineering from SIIT, Bangkok, Thailand, in 1999, the M.E. degree in computer engineering from KMUTT, Bangkok, in 2001, the M.S. degree in electrical engineering from Boston University, Boston, MA, USA, in 2006, and the Ph.D. degree in computer engineering from Northeastern University, Boston, MA, USA, in 2013.

Currently, he is a Lecturer in the Computer Engineering Department at Rajamangala University of Technology Thanyaburi, Thailand. His expertise and research interests lie in RF energy harvesting circuit design, protocol design in energy harvesting wireless sensor networks, and ultra-low power wireless sensor networks.

Dr. Nintanavongsa won a best paper award at the IEEE ICNC conference in 2013. He was a recipient of the Royal Thai government scholarship.

Kaushik R. Chowdhury (M'09) received the B.E. degree in electronics engineering with distinction from VJTI, Mumbai University, India, in 2003, the M.S. degree in computer science from the University of Cincinnati, Cincinnati, OH, USA, in 2006, and the Ph.D. degree from the Georgia Institute of Technology, Atlanta, GA, USA, in 2009.

He is Assistant Professor in the Electrical and Computer Engineering Department at Northeastern University, Boston, MA, USA. He currently serves on the editorial board of the Elsevier *Ad Hoc Networks* and Elsevier *Computer Communications* journals. His expertise and research interests lie in wireless cognitive radio *ad hoc* networks, energy harvesting, and intra-body communication.

Dr. Chowdhury is the recipient of multiple best paper awards at the IEEE ICC conference. His M.S. thesis was given the outstanding thesis award jointly by the Electrical and Computer Engineering and Computer Science Departments at the University of Cincinnati, Cincinnati.